Nanoscale

Accepted Manuscript

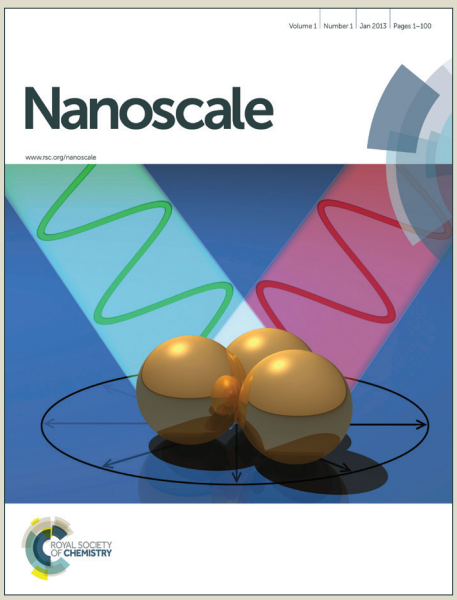

ROYAL SOCIETY OF CHEMISTRY

www.rsc.org/nanoscale

Charge Transfer between Carbon Nanotubes on Surfaces

Karolline A.S. Araujo[†,‡], Ana P.M. Barboza[†], Thales F. D. Fernandes[†], Nitzan Shadmi[§], Ernesto Joselevich[§], Mario S. C. Mazzoni[†] and Bernardo R.A. Neves[†]*

[†]Departamento de Física, ICEx, Universidade Federal de Minas Gerais, Belo Horizonte, Brazil, [‡]Instituto Federal de Minas Gerais, Ponte Nova, Brazil and [§]Department of Materials and Interfaces, Weizmann Institute of Science, Rehovot, Israel.

* Corresponding author email: bernardo@fisica.ufmg.br

Abstract

The charge transfer between neighboring single-wall carbon nanotubes (SWNTs) on silicon oxide surface was investigated as a function of both SWNT nature (metallic or semiconducting) and anode/cathode distance using scanning probe techniques. Two main mechanisms were observed: a direct electron tunneling described by the typical Fowler–Nordheim model, and an indirect electron transfer (hopping) mediated by functional groups on the supporting surface. Both mechanisms depend on SWNT nature and on anode/cathode separation: direct electron tunneling dominates the charge transfer process for metallic SWNTs, especially for large distances, while both mechanisms compete with each other for semiconducting SWNTs, prevailing one over the other depending on the anode/cathode separation. These mechanisms may significantly influence the design and operation of SWNT-based electronic devices.

Introduction

Charge transfer is a fundamental process in nanoscale systems, ranging from the DNA oxidative damage, which is critical to the viability of all living organisms, to the performance of ultimate electronics[1,2]. Its understanding may even open up completely new directions of research, such as DNA- or carbon nanotube-based electronics[1,3]. Therefore, its thorough investigation is necessary before any new material may become a real commodity for the electronics industry. Single-wall carbon nanotubes (SWNTs) are a class of materials that have been the subject of intense investigation for more than two decades due to the large range of possible applications they provide to nanotechnology[4–6]. Many different electronic devices, such as field-effect transistors and diodes, using SWNTs as core elements, were proposed and demonstrated[4]. Their high aspect ratio was explored in proof-of-concept studies, which illustrated their viability as high-efficiency electron emitters[4–7], working as efficient and inexpensive field emission sources for flat panel displays, microwave generators and X-ray tubes[8,9]. Taking further advantage of their 1D nature and high conductivity, SWNTs were employed, likewise, as wire interconnects in nano-sized electronics circuits[10]. For many such possible applications, a key physical process affecting their electric/electronic usage is the mechanism of eventual charge transfer between neighboring SWNTs resting on a surface. In this context, some works investigated the charge transfer on a nanotube network (NTN), where each nanotube is in direct physical contact (no gap between them) with its neighboring nanotube[11-14]. The resistance on such NTNs is related to charge transfer effects at the junctions formed by crossed semiconducting/ semiconducting, or metallic/metallic, or semiconducting/metallic nanotubes[11]. Despite its obvious importance for SWNT-based nanodevices and mainly due to the significant difficulty in their manipulation, no studies of charge transfer between non-connected (with a physical gap) and isolated SWNTs on a surface have been developed and only a few, employing suspended carbon nanotubes, have been reported[4,15]. Here, we address the challenge of investigating the charge transfer between isolated nanotubes after their nanomanipulation by microscopic techniques. A new experimental setup is utilized, in which isolated SWNTs resting on a Si oxide surface are cut and displaced, so that one half works as cathode, after being charged, and the other as an anode. Using Scanning Probe Microscopy (SPM) electrical characterization and nanomanipulation, the charge transfer

between neighboring SWNTs is monitored as a function of nanotube nature (metallic or semiconducting) and anode/cathode distance.

Experimental

Isolated SWNTs were grown atop the Si oxide substrate via chemical vapor deposition (CVD) synthesis[16]: Si/SiO_2 (Si (100) with a thermal oxide layer of 200 nm, purchased from International Wafer Service Inc.) wafers were cut to samples, roughly 8 × 8 mm^2 in size. Samples were cleaned by sonication in acetone for 10 min, followed by rinsing in acetone and isopropanol, and drying by N_2. Parallel stripes (25 μm wide, 25 nm thick) of amorphous SiO_2 (Kurt J. Lesker, 99.99%), followed by a thin layer (nominally 0.3 nm) of Fe (Kurt J. Lesker, 99.95%) growth catalyst were deposited on the substrate by standard photolithography and electron-beam evaporation. Lift-off was done in acetone. The samples were introduced into a tube furnace (Lindberg blue) and aligned such that the catalyst stripes were roughly perpendicular to the gas flow direction. The samples were heated at 550 °C for 20 min in air to remove organic contaminations. Single-wall carbon nanotubes were then grown by CVD: samples were heated to 900 °C, in an atmosphere of 60% Ar (Oxygen & Argon Industries, 99.996%) and 40% H_2 (Gordon Gas, 99.999%), followed by introduction of ~0.2% C_2H_4 (Gordon Gas, 99.9%). The total flow rate was 1000 sccm for a growth time of 45 minutes. At the end of the growth time, samples were left to cool in Ar.

All measurements were performed using either a Nanoscope V MultiMode SPM from Bruker or a XE-70 SPM from Park Instruments. Atomic Force Microscopy (AFM) was employed to cut isolated SWNTs and to manipulate the distance between the created anode/cathode elements. Electrostatic Force Microscopy (EFM) techniques were used to sort out metallic from semiconducting SWNTs[17,18] and to inject and measure their charge[19]. Charge transfer experiments were carried under dry nitrogen environment to reduce nanotube discharge to the atmosphere during the measurements. Isolated SWNTs were cut by diamond-like carbon (DLC)-coated silicon cantilevers from NT-MDT with nominal spring constant k ~ 48 N/m, nominal radius of curvature R ~ 50 nm and nominal resonant frequency 420 kHz to form both anode and cathode elements. Two types of doped silicon cantilevers from Nanosensors with nominal spring constants k ~ 42 and 2.8 N/m, nominal

resonant frequency 330 and 75 kHz, respectively, and nominal radius of curvature R ~ 10 nm (both) were employed throughout this work on nanomanipulation and electric experiments.

Aligned SWNTs, characterized via AFM imaging, showed uniform diameters ~1.2nm. Their electric nature (metallic or semiconducting) was identified via the EFM line profile method[17,18]. Once the electric nature of a SWNT was known, the steps illustrated in Figure 1 were carried out: In step (a), the nanotube is cut by the AFM tip into two parts, forming the anode/cathode elements separated by a distance d. Then, in step (b) - charge injection procedure, the tip is put in contact with one of the nanotube halves (cathode) with an applied bias V, charging it[19]. In step (c), the injected charge density on the cathode (λ) and the possible transferred charge density to the anode (λ') are measured via regular EFM imaging with no applied bias to the tip[19]. Finally, in step (d), the AFM tip pushes (or pulls) a nanotube end, varying the anode-cathode distance d and steps (b) and (c) are repeated. Figure 2 illustrates the whole process schematized in Fig.1. The inset in Fig. 2a shows the AFM image of a SWNT cut into two pieces (step (a) on Fig. 1). Figures 2a and 2b show typical EFM images of the charging process, without (Fig. 2a) or with (Fig. 2b) charge transfer between the nanotubes. For a small amount of injected charges on the cathode nanotube (low bias V_{tip} on Fig. 1b), no charge is transferred to the anode nanotube (Fig. 2a). On the other hand, for large charge injection on the cathode (large bias V_{tip} on Fig. 1b), a significant charge amount is transferred to the neighboring nanotube (which becomes visible on the EFM image - Figure 2b - and is a signature of charge transfer between SWNTs).

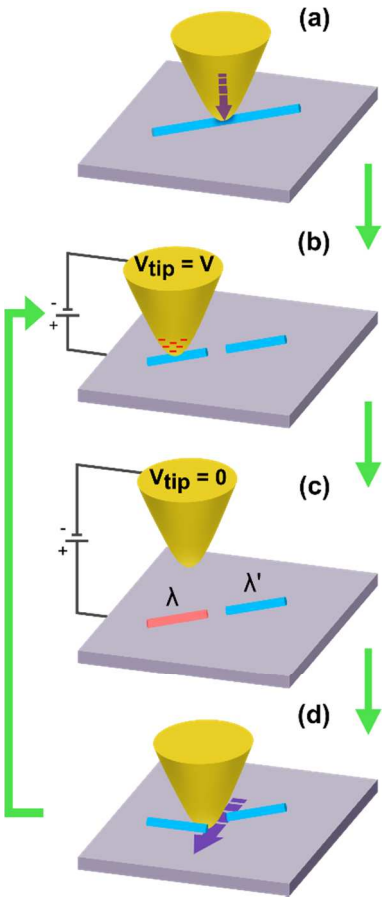

Figure 1. Nanomanipulation and charge transfer experiments. The experimental steps are: (a) cutting of isolated SWNT with the AFM tip; (b) charge injection procedure; (c) EFM charge density measurement (with no applied bias) and; (d) nanomanipulation of the cut nanotube.

During the experiment, steps (b) and (c) of Fig. 1 are repeated several times for a given SWNT separation distance in order to acquire different pairs of injected charge density on cathode (λ) and transferred charge density to the anode (λ') by varying the injection tip bias[19]. It is important to emphasize that each charge injection process is carried out with the anode nanotube totally discharged to avoid any influence on the data. Subsequently, the distance between SWNTs is varied via AFM nanomanipulation (Fig.1d) and steps (b) and (c) are repeated over again in this new configuration. Figures 2c and 2d exemplify a typical AFM nanomanipulation of the anode/cathode SWNT distance.

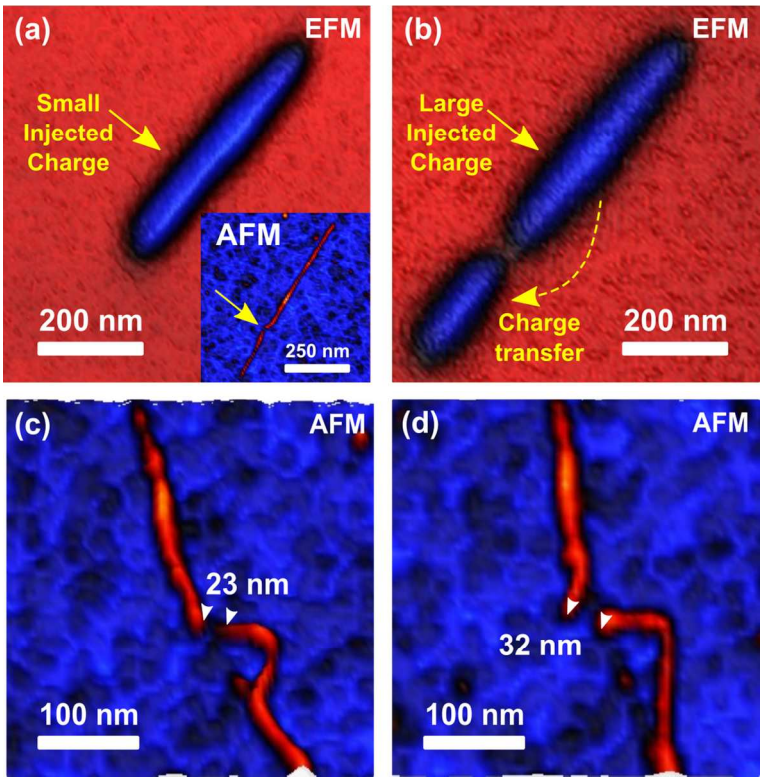

Figure 2. (a) EFM image for small injected charge reveals that no charge was transferred to the neighboring nanotube, making it invisible in the EFM image. The inset shows the AFM image of the cut anode/cathode SWNT elements. (b) For large injected charge, the anode nanotube becomes visible, showing that the charge transfer between cathode/anode took place. The distances between the cathode/anode SWNTs before and after a manipulation are displayed on (c) and (d), respectively.

The Fowler-Nordheim (FN) model, extensively employed in the field emission context[5–7,20,21], can also be employed to analyze the charge transfer process evidenced in the EFM images of the present work. Within the FN theory, the characteristic current density J from the emitter to the collector depends on the emitter electric field E following equation (1) below, where a and b are constants that depend on the work function of the emitter[21,22]. Usually, in field emission analysis, eq. (1) is written in the linearized form $ln(J/E^2) = -(b/E) + ln(a)$[5–7,20,21].

$$J = aE^2\exp((-b)/E) \quad (1)$$

Within the field emission framework, SWNT structural properties, particularly the cylindrical shape of its body and its small tip radius are important parameters that directly influence the cathode emission process[23,24]. The tip-end of SWCNTs can be modeled as a hemisphere and the local electrical field relates to the nanotube tip radius as: $E = V/\zeta R_{tip}$, where R_{tip} is the tip radius of curvature and ζ is a modifying factor determined by local geometric and electronic factors[25,26]. Then, according to eq. (1), the emission decays exponentially with the nanotube tip radius R_{tip}, i.e., sharper tips yield higher current densities. Therefore, in the present work, the small diameter of SWCNTs indicates a small tip radius, which suggests they should produce a considerable field amplification factor and, thus, should behave as good emission sources[27,28].

Theoretical work has also demonstrated that the work function of SWCNTs can vary considerably from 5.44 eV (closed) to 4.86 eV (open-ended)[29]. This variation leads to an increase on the slope (the linearized form of the eq. (1)) in the FN plot of open-ended nanotubes compared with the closed nanotubes, indicating an enhancement on field emission properties[29]. Additionally, experiments[28,30] and simulations[28] have shown that the local density of states at the tip presents sharp localized states that are correlated to the presence of pentagonal defects and, therefore, SWNTs cannot be considered as conventional metallic emitters[27]. Since the largest part of emitted current comes from occupied states close to the Fermi level, the emission behavior (increase/decrease on the slope or threshold field to initiate the emission) is affected by the tip radius geometry (i.e., the tube chirality, diameter and the presence of defects)[27,28]. Nevertheless, in a good approximation, the simplified FN form (eq. (1)) can be applied both for metallic and semiconducting SWNTs with small diameters[31].

Since the electric field at the emitter nanotube (electric field of a charged wire) is proportional to its injected charge density ($E \propto \lambda$)[19] and the emission current is also proportional to the transferred charge density ($J \propto \lambda'$), it is convenient to analyze the present results in terms of charge densities λ and λ' measured in the EFM experiments. Therefore, the FN expression can be re-written, in a linearized form, as equation (2) below, with A and B being arbitrary constants. As a consequence, a plot of $ln(\lambda'/\lambda^2)$ versus $(1/\lambda)$

which yields negative-slope lines can be considered as a signature of the FN regime during charge transfer.

$$ln(\lambda'/\lambda^2) = ln(A) - (B/\lambda), \quad (2)$$

In view of the above discussion, Figures 3a and 3b show plots of the quantity $ln(\lambda'/\lambda^2)$ versus $(1/\lambda)$ for metallic and semiconducting SWNTs, respectively. More precisely, Fig. 3a shows typical results for a metallic nanotube with different cathode/anode distances. The apparent linear behavior with negative slopes demonstrate the applicability of the FN mechanism (eq. 2) in this case, regardless the cathode/anode distance. In other words, there is an indication of the FN regime in the charge transfer between metallic nanotubes. It should be noted that, interestingly, the slopes are less pronounced for decreasing distances.

On the other hand, as Fig. 3b shows, semiconducting SWNTs clearly present two different behaviors depending on the cathode/anode distance. For large distances (blue-colored symbols), the apparent linear dependence with negative slope suggests again the validity of the FN approach. However, for small distances (green-colored symbols), $ln(\lambda'/\lambda^2)$ becomes an increasing function of $1/\lambda$, indicating the emergence of a distinct mechanism governing the charge transfer between semiconducting nanotubes.

Another interesting parameter in the transfer process is the charge density threshold λ_T, which is the necessary charge density at the emitter nanotube to initiate the charge transfer process to its neighboring nanotube. Hence, Figure 3c shows the influence of the cathode-anode distance on the charge density threshold λ_T for both metallic and semiconducting SWNTs. For metallic nanotubes (green diamonds on Fig. 3c), λ_T weakly depends on the cathode/anode separation. However, for semiconducting nanotubes (blue circles), Figure 3c clearly shows that, in fact, a second mechanism, involving lower density thresholds, operates at small distances. For larger distances (d > 60 nm), the behavior of semiconducting nanotubes approaches that of metallic ones. Finally, using λ_T to calculate the electric field threshold E_T, it is worth noting that the macroscopic field on a nanotube end ($E_T \sim 6.3$ -7.9 $V/\mu m$) found in this work is comparable to the typical threshold field ($E_T = 3.9 - 7.8\ V/\mu m$) to produce a field-emission current of 10 $mAcm^{-2}$ for SWNTs[32].

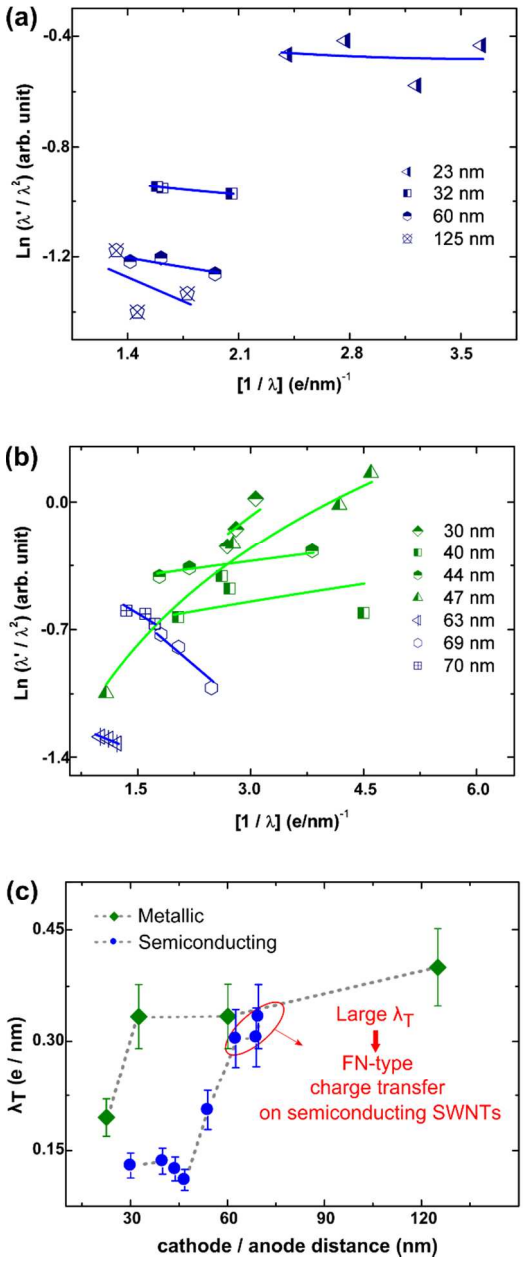

Figure 3. The charge transfer mechanism between SWNTs is characterized via plots of $\ln(\lambda'/\lambda^2)$ versus $1/\lambda$, where λ (λ') is the injected (transferred) linear charge density (measured in e/nm), for metallic (a) and semiconducting (b) nanotubes. The full lines (blue and green) in both plots are fits with eq. (4). (c) Graph of the charge density threshold λ_T to initiate charge transfer to the anode for metallic (green diamonds) and semiconducting (blue circles) SWNTs.

The results of figs. 3b and 3c indicate that the FN model (eq. 2) alone is not enough to explain all experimental data. There might be an additional charge transfer process assisting, or competing with, the FN one. In other words, a more complete model is needed in order to analyze the experimental results above. In such model, the current density *J* leading to the charge transfer between neighboring SWNTs resting on a dielectric surface might be modeled as electron tunneling based on two main mechanisms. The first one is a direct process, from one nanotube to the other, viewed as conventional electron tunneling between two regions separated by an energy barrier. In such cases, the well-known Tsu-Esaki formula assumes a parabolic electronic dispersion in both regions and yields the current density *J* as an energy integral involving the product of a transmission function and a supply function, which carries information about the electronic occupancy distributions[33]. In the limit of larger separations, it is reasonable to assume a triangular shape for the energy barrier and, thus, the Tsu-Esaki expression leads directly to the Fowler-Nordheim eq. (1)[21].

Functional chemical groups in the Si oxide surface may mediate an additional possible mechanism. Figure 4 illustrates this hypothesis and Figs. 4a and 4b (inset) portray two relaxed models for crystalline SiO_2 surfaces in which the dangling bonds are saturated by hydrogen atoms, generating silanols, geminal silanols and associated silanol groups. Figure 4b shows the density of states (DOS) for the model shown in the inset, calculated within the density functional theory formalism framework[34–39], exhibiting the higher occupied and lower unoccupied states with a projection that highlights the contribution of all silanol groups. A relatively high energy tunneling barrier is expected in this case due to the large SiO_2 gap energy, which may be considerably decreased if we consider that the actual substrate is amorphous and may present defects responsible for the introduction of states in the gap region. Independent of the specific model, the small distance between adjacent groups (0.2 to 0.5 nm), when compared to the inter-nanotube distance (20 to 60 nm), makes this second mechanism competitive when the density of states of the collector nanotube (anode) also vanishes, that is, in the case of semiconducting nanotubes. Such small distances also allow us to assume a negligible energy variation in the energy barrier profile as opposed to the triangular shape of the FN model, which leads to a constant transmission function, implying a linear response[40].

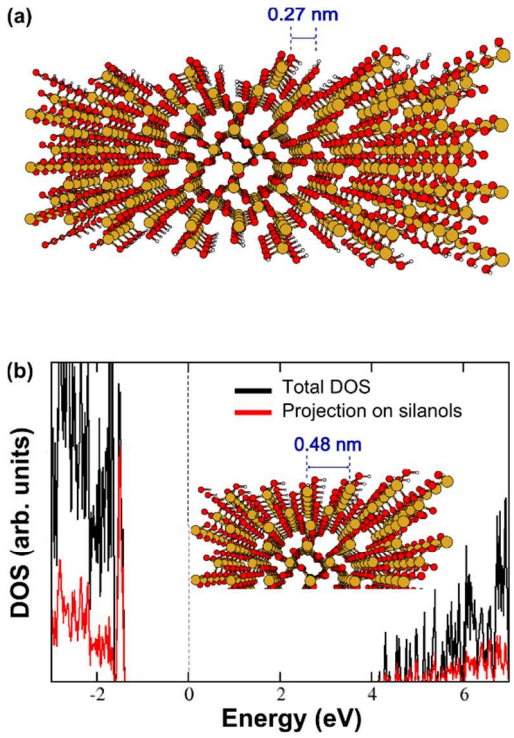

Figure 4. Qualitative aspects of the model employed to analyze the charge transfer mechanisms between neighboring nanotubes. (a) Relaxed model for a crystalline SiO_2 surface and (b) the calculated density of states of a specific crystalline SiO_2 surface (insert).

Therefore, the charge transfer between surface functional groups separated by a distance d_0 should follow a hopping transport scheme[41,42] with individual resistances proportional to $R_0 e^{\beta d_0}$, where R_0 and β are constants. Adding the individual resistances, the total resistance in a inter-nanotube distance d should be proportional to $dR_0 e^{\beta d_0}$. This hopping process, being linear, has, as signature, a constant conductivity $J_h = \sigma_h E$. Finally, this second mechanism is expected to vanish in large separations due to increased resistance and isotropic charge dissipation. In order to take this last effect into account, the contribution of the second mechanism should be weighted by an exponential decreasing factor as a function of the intertube distance ($e^{-\alpha d}$, where α is a constant). Therefore, equation 3 summarizes the complete model:

$$ln\left(\frac{J}{E^2}\right) = \ln\left[e^{-b(1/E)} + \sigma_h\left(\frac{1}{E}e^{-\alpha d}\right)\right] \quad (3)$$

Similarly to eqs. (1) and (2), eq. (3) can be re-written in terms of the experimental quantities λ and λ' as

$$ln\left(\frac{\lambda\prime}{\lambda^2}\right) = ln\left(Ae^{-B/\lambda} + \frac{C}{\lambda}\right) \quad (4)$$

In eq. (4), A, B and C are fitting parameters where B is directly related to the slope in the FN model (direct tunneling) and C is associated with the indirect (hopping) process. In order to test the validity of the complete model, all experimental data in figs. 3a and 3b were fit with eq. 4 (full lines in figs. 3a and 3b). The good qualitative agreement between theory and experiment is evident, indicating the validity of the complete model assumptions. Moreover, the quantitative analysis of the fitting parameters A, B and C brings further support to the hypothesis of a transition between two charge transfer regimes for semiconducting nanotube suggested by fig. 3c. Table 1 shows the values of A, B and C for all experimental data in figs. 3a (metallic SWNTs) and 3b (semiconducting SWNTs).

Table 1 – Fitting parameters of eq. (4) for the experimental data in figures 3a (metallic SWNTs) and 3b (semiconducting SWNTs).

METALLIC			
Distance (nm)	A	B	C
23	0.76	0.22	0.08
32	0.45	0.22	0.05
60	0.36	0.21	0.03
125	0.39	0.25	0.0001
SEMICONDUCTING			
Distance (nm)	A	B	C
30	0.09	0.0001	0.28
40	0.46	0.0001	0.04
44	0.61	0.0001	0.04
47	0.14	0.0001	0.21
63	0.32	0.17	0.0001
69	0.89	0.35	0.0001
70	0.79	0.25	0.0001

As discussed above, parameter B characterizes the FN regime (direct tunneling), whereas parameter C describes the hopping (indirect) process. Analyzing metallic SWNTs first, it is evident that the FN parameter B dominates the hopping parameter C, even though C shows non-zero values. It should be pointed, though, that fitting the experimental data for metallic SWNTs with eq. (2), which considers the FN model only, produces a linear fitting that is essentially undistinguishable from the one obtained with eq. (4) (data not shown). Therefore, even observing non-zero values for the hopping parameter C, the charge transfer between metallic nanotubes is definitely governed by the FN regime, in agreement with the initial qualitative interpretation of fig. 3a. However, the most striking result in Table 1 is observed for the case of semiconducting SWNTs: initially, for small inter-tube distances, the hopping parameter C is the most significant, with the FN parameter B being vanishingly small. A sharp transition is observed at larger distances (> 60nm), when the hopping parameter C vanishes and the FN parameter B dictates the behavior. Such result is in excellent agreement with the hypothesis extracted from the data in fig. 3c for the charge density threshold λ_T to initiate the charge transfer process between nanotubes. In other words, the fitting of the experimental data of fig. 3b with the model of eq. (4) independently indicates a transition between two leading charge transfer mechanisms in semiconducting SWNTs: at short distances, indirect and substrate-mediated charge transfer occurs, whereas, at larger distances, direct tunneling is the main transfer mechanism.

In conclusion, this work investigates the charge transfer between SWNTs on a supporting substrate via SPM nanomanipulation and electric characterization. The experimental data for metallic and semiconducting nanotubes strongly suggest the occurrence of two distinct mechanisms: (1) charge transfer between neighboring metallic SWNTs occurs via direct FN quantum tunneling mechanism; and (2) for semiconducting SWNTs, charge transfers via a hopping-type indirect process for small distances and a direct FN tunneling process for larger distances. Moreover, for metallic nanotubes, the charge density threshold λ_T weakly depends on the anode/cathode separation, while for semiconducting nanotubes, there is a stronger dependence with the distance, indicating two charge transfer regimes. This result could have general implications to other systems. For instance, charge transfer along DNA is also governed by these same two regimes: tunneling and hopping[1]. However, unlike the observed SWNT behavior, tunneling is the leading

charge transfer mechanism for short distances, whereas hopping controls charge transport along larger distances[1]. Interestingly, nevertheless, a recent work also shows the coexistence of both hopping and tunneling regimes for intermediate distances along DNA, in close similarity to the findings of the present work[43]. In other words, the occurrence of distinct and competing mechanisms of charge transport may be a general property of low-dimensional systems at the nanoscale.

References

1 J. C. Genereux and J. K. Barton, *Chem. Rev.*, 2010, 110, 1642–1662.

2 K. F. Brennan and A. S. Brown, *Theory of modern electronic semiconductor devices*, John Wiley, 2002.

3 N. C. Seeman, *Annu. Rev. Biochem.*, 2010, 79, 65–87.

4 A. Jorio, G. Dresselhaus and M. S. Dresselhaus, *Carbon Nanotubes: Advanced Topics in the Synthesis, Structure, Properties and Applications*, Springer Science & Business Media, 2007.

5 A. G. Rinzler, J. H. Hafner, P. Nikolaev, P. Nordlander, D. T. Colbert, R. E. Smalley, L. Lou, S. G. Kim and D. Tománek, *Science*, 1995, 269, 1550–1553.

6 W. A. de Heer, A. Ch telain and D. Ugarte, *Science*, 1995, 270, 1179–1180.

7 Y. Saito, K. Hamaguchi, K. Hata, K. Uchida, Y. Tasaka, F. Ikazaki, M. Yumura, A. Kasuya and Y. Nishina, *Nature*, 1997, 389, 554–555.

8 A. M. Rao, D. Jacques, R. C. Haddon, W. Zhu, C. Bower and S. Jin, *Appl. Phys. Lett.*, 2000, 76, 3813.

9 Y. Saito and S. Uemura, *Carbon*, 2000, 38, 169–182.

10 M. S. Fuhrer, *Science*, 2000, 288, 494–497.

11 P. N. Nirmalraj, P. E. Lyons, S. De, J. N. Coleman and J. J. Boland, Nano Lett., 2009, 9, 3890–3895.

12 M. Stadermann, S. J. Papadakis, M. R. Falvo, J. Novak, E. Snow, Q. Fu, J. Liu, Y. Fridman, J. J. Boland, R. Superfine and S. Washburn, Phys. Rev. B, 2004, 69, 201402.

13 A. Fujiwara, R. Iijima, K. Ishii, H. Suematsu, H. Kataura, Y. Maniwa, S. Suzuki and Y. Achiba, Appl. Phys. Lett., 2002, 80, 1993.

14 M. Stadermann, S. J. Papadakis, M. R. Falvo, Q. Fu, J. Liu, Y. Fridman, J. J. Boland, R. Superfine and S. Washburn, Phys. Rev. B, 2005, 72, 245406.

15 F. Arai, P. L. P. Liu, L. D. L. Dong and T. Fukuda, *IEEE Int. Conf. Robot. Autom. 2004. Proceedings. ICRA '04. 2004*, 2004, 1, 597–603.

16 N. Shadmi, N. Geblinger, A. Ismach and E. Joselevich, *J. Phys. Chem. C*, 2014, 118, 14044–14050.

17 A. P. M. Barboza, A. P. Gomes, H. Chacham and B. R. A. Neves, *Carbon*, 2010, 48, 3287–3292.

18 J. S. Soares, A. P. M. Barboza, P. T. Araujo, N. M. Barbosa Neto, D. Nakabayashi, N. Shadmi, T. S. Yarden, A. Ismach, N. Geblinger, E. Joselevich, C. Vilani, L. G. Cançado, L. Novotny, G. Dresselhaus, M. S. Dresselhaus, B. R. A. Neves, M. S. C. Mazzoni and A. Jorio, *Nano Lett.*, 2010, 10, 5043–5048.

19 A. P. M. Barboza, A. P. Gomes, B. S. Archanjo, P. T. Araujo, A. Jorio, A. S. Ferlauto, M. S. C. Mazzoni, H. Chacham and B. R. A. Neves, *Phys. Rev. Lett.*, 2008, 100, 1–4.

20 X. Zheng, G. Chen, Z. Li, S. Deng and N. Xu, *Phys. Rev. Lett.*, 2004, 92, 106803–1.

21 J. W. Gadzuk and E. W. Plummer, *Rev. Mod. Phys.*, 1973, 45, 487–548.

22 V. Filip, D. Nicolaescu and F. Okuyama, *J. Vac. Sci. Technol. B Microelectron. Nanom. Struct.*, 2001, 19, 1016.

23 J. Bonard, F. Maier, T. Stöckli, A. Châtelain, W. A. de Heer, J. Salvetat and L. Forró, Ultramicroscopy, 1998, 73, 7–15.

24 Q. H. Wang, T. D. Corrigan, J. Y. Dai, R. P. H. Chang and a. R. Krauss, Appl. Phys. Lett., 1997, 70, 3308.

25 R. Gomer, Field Emission and Field Ionization, Harvard University Press, Cambridge, 1961, 195.

26 P. G. Collins and a. Zettl, Phys. Rev. B, 1997, 55, 9391–9399.

27 J.M. Bonard, J.P. Salvetat, T. Stöckli, L. Forró and A. Châtelain, Appl. Phys. A Mater. Sci. Process., 1999, 69, 245–254.

28 D. L. Carroll, P. Redlich, P. M. Ajayan, J. C. Charlier, X. Blase, A. De Vita and R. Car, Phys. Rev. Lett., 1997, 78, 2811–2814.

29 G. Zhou, W. Duan and B. Gu, Phys. Rev. Lett., 2001, 87, 095504.

30 J.M. Bonard, T. Stöckli, F. Maier, W. A. de Heer, A. Châtelain, J.-P. Salvetat and L. Forró, Phys. Rev. Lett., 1998, 81, 1441–1444.

31 Shi Dong Liang and Lu Chen, Phys. Rev. Lett., 2008, 101, 027602.

32 J.M. Bonard, J.P. Salvetat, T. Stöckli, W. A. de Heer, L. Forró and A. Châtelain, *Appl. Phys. Lett.*, 1998, 73, 918.

33 R. Tsu and L. Esaki, *Appl. Phys. Lett.*, 1973, 22, 562–564.

34. We employed the SIESTA implementation with a double-zeta basis set augmented by poarization functions, Troullier-Martins pseudopotentials in the Kleinman-Bylander form and the generalized gradient approximation in the Perdew-Burke-Ernzerhof parametrization.

35 W. Kohn and L. J. Sham, *Phys. Rev.*, 1965, 140, A1133.

36 N. Troullier and J. L. Martins, *Phys. Rev. B*, 1991, 43, 8861–8869.

37 L. Kleinman and D. M. Bylander, *Phys. Rev. Lett.*, 1982, 48, 1425–1428.

38 J. M. Soler, E. Artacho, J. D. Gale, A. Garcia, J. Junquera, P. Ordejon and D. Sanchez-Portal, *J. Phys. Condens. Matter*, 2002, 2745, 35.

39 J. P. Perdew, K. Burke and M. Ernzerhof, *Phys. Rev. Lett.*, 1996, 77, 3865–3868.

40 S. Datta, *Electronic Transport in Mesoscopic Systems*, Cambridge University Press, 1997.

41 B. I. Shklovskii and A. L. Efros, *Electronic properties of doped semiconductors*, Springer Berlin Heidelberg, 1984.

42 A. Aparecido-Ferreira, G. M. Ribeiro, E. S. Alves and J. F. Sampaio, *Phys. Rev. B - Condens. Matter Mater. Phys.*, 2011, 84, 1–6.

43 L. Xiang, J. L. Palma, C. Bruot, V. Mujica, M. A. Ratner and N. Tao, *Nat. Chem.*, 2015, 7, 221–226.